GEOLOGICA CARPATHICA, FEBRUARY 2015, 66, 1, 3–17 doi: 10.1515/geoca-2015-0007

Geochemistry and Sr, Nd isotopic composition of the Hronic Upper Paleozoic basic rocks (Western Carpathians, Slovakia)

JOZEF VOZÁR[1], JÁN SPIŠIAK[2], ANNA VOZÁROVÁ[3], JAKUB BAZARNIK[4] and JÁN KRÁĽ[5]

[1]Geological Institute of Slovak Academy of Sciences, Dúbravská cesta 9, P.O. Box 106, 840 05 Bratislava, Slovak Republic; jozef.vozar@savba.sk
[2]Faculty of Natural Sciences, Matej Bell University, Tajovského 40, 974 01 Banská Bystrica, Slovak Republic; jan.spisiak@umb.sk
[3]Faculty of Natural Sciences, Comenius University, Mlynská dolina, 842 15 Bratislava, Slovak Republic; vozarova@fns.uniba.sk
[4]Polish Geological Institute — National Research Institute, Rakowiecka 4, 00-975 Warszawa, Poland; jakub.bazarnik@pgi.gov.pl
[5]Dionýz Štúr State Geological Institute, Mlynská dolina 1, 817 04 Bratislava, Slovak Republic; jan.kral.ba@gmail.com

(Manuscript received July 14, 2014; accepted in revised form December 10, 2014)

Abstract: The paper presents new major and trace element and first Sr-Nd isotope data from selected lavas among the Permian basaltic andesite and basalts of the Hronicum Unit and the dolerite dykes cutting mainly the Pennsylvanian strata. The basic rocks are characterized by small to moderate $mg^{\#}$ numbers (30 to 54) and high SiO_2 contents (51–57 wt. %). Low values of TiO_2 (1.07–1.76 wt. %) span the low-Ti basalts. Ti/Y ratios in the dolerite dykes as well as the basaltic andesite and basalt of the 1st eruption phase are close to the recommended boundary 500 between high-Ti and low-Ti basalts. Ti/Y value from the 2nd eruption phase basalt is higher and inclined to the high-Ti basalts. In spite of this fact, in all studied Hronicum basic rocks Fe_2O_3* is lower than 12 wt. % and Nb/La ratios (0.3–0.6) are low, which is more characteristic of low-Ti basalts. The basic rocks are characterized by Nb/La ratios (0.56 to 0.33), and negative correlations between Nb/La and SiO_2, which point to crustal assimilation and fraction crystallization. The intercept for Sr evolution lines of the 1st intrusive phase basalt is closest to the expected extrusions age (about 290 Ma) with an initial $^{87}Sr/^{86}Sr$ ratio of about 0.7054. Small differences in calculated values I_{Sr} document a partial Sr isotopic heterogeneity source (0.70435–0.70566), or possible contamination of the original magma by crustal material. For Nd analyses of the three samples, the calculated values εCHUR (285 Ma) are positive (from 1.75 to 3.97) for all samples with only subtle variation. Chemical and isotopic data permit us to assume that the parental magma for the Hronicum basic rocks was generated from an enriched heterogeneous source in the subcontinental lithospheric mantle.

Key words: Western Carpathians, Hronicum Unit, Permian volcanics, geochemistry, Sr and Nd isotopic composition.

Introduction

Hronicum, as a rootless multi-nappe unit in the tectonic structure of the Inner Western Carpathians, is characterized by dominant Carboniferous/Permian volcanic-sedimentary sequences defined by Vozárová & Vozár (1981, 1988) as the Ipoltica Group. The Ipoltica Group (IG) is subdivided into the Nižná Boca Formation (NBF — Late Pennsylvanian) and Malužiná Formation (MF — Permian). Stratigraphic interpretation from both lithostratigraphic units is based on lithology, palynology, macroflora and sporadically isotopic/radiometric evidence.

The paper presents Nd and Sr isotopic data and the results of geochemical study of Permian Hronicum basic volcanics and the associated system of subvolcanic doleritic dykes and sills. The aim of our research was to detect the main isotopic differences between individual volcanic eruption phases and the similarity of subvolcanic dolerite dykes and sills. It can be considered that Sr and Nd isotopes keep a record of geological evolution (e.g. Allègre 2008) and thus, the isotopic compositions of the studied volcanic and subvolcanic basic rocks could contribute to the interpretation of the magma genesis, the position of the magma chamber in relation to the continental crust and upper mantle. Consequently, they can solve the relationships between individual phases of volcanism in relation to basin evolution and individual phases of rifting.

For precise determination of the geological position of volcanic bodies and their stratigraphic stage more comprehensive information is needed. The main topics of our research were focused on:

1. Stratification and genetic interpretation of the basic volcanic rocks of the Hronicum Unit in relation to basin evolution and its paleotectonic setting, with the use of Sm-Nd and Sr-Sr isotope analyses;

2. The genetic relation of dykes in the Late Pennsylvanian NBF — if they are related to the beginning of rifting or they are comagmatic with Permian basalts.

In an effort to contribute to the solution of these problems, we collected samples from a dolerite dyke (sample NT-1), from the 1st eruption phase basaltic andesite and basalt (samples Ip-1 and NT-2) and from of the 2nd eruption phase basalts (samples Kv-2 and NT-3) for $^{87}Sr/^{86}Sr$ and Nd-Sm isotope analyses. The results are the first ever isotope data from the Hronicum Late Paleozoic basic rocks.

Geological setting

The Hronicum Unit represents a system of higher nappes which were characterized as the so-called rootless nappes (lower *Šturec* nappe, higher *Choč* nappe — Biely & Fusán

1967; Andrusov 1968; Andrusov et al. 1973). From the base to the upper part, the Hronicum is composed of Upper Pennsylvanian to Jurassic members. In the present-day structure of the Western Carpathians, the Upper Paleozoic of the Hronicum Unit are mainly preserved in the basal part of the lower (Šturec) nappe. It may be delimited in various areas of the Western Carpathians territory (from the pre-Tertiary basement of the Vienna Basin and the Malé Karpaty Mts in the west as far as the Branisko and Sľubica Mts in the east, from the Malá Fatra Mts and basement of the Liptovská kotlina and Hornádska kotlina depressions in the north to the Southern Veporicum in the Stolické vrchy Mts) in the south. The best preserved fragments of the Upper Paleozoic IG have been described from the Nízke Tatry Mts (lithostratigraphic type profiles along the Ipoltica valley and near Nižná Boca and Malužiná villages).

The Upper Paleozoic lithostratigraphy of the Hronicum is presented by two formations — the NBF (Late Pennsylvanian) and MF (Permian), belonging to the IG (Vozárová & Vozár 1981, 1988). The age of both formations is confirmed by findings of the uppermost Pennsylvanian macroflora (Sitár & Vozár 1973), Upper Pennsylvanian/Permian microflora (Ilavská 1964; Planderová 1973, 1979) and scarce radiometric U-Pb dating of uranium U-mineralization (Rojkovič 1975, 1997 — Kravany beds 263–274 Ma). The 310–340 Ma age of the presumed source area was indicated by the $^{40}Ar/^{39}Ar$ dating of detrital mica from sandstones (Vozárová et al. 2005), which suggests the age of the IG sedimentary basin younger than 310 Ma. The position of the IG sedimentary sequence in the underlier of the Lower Triassic Benkovský potok Formation (sensu Biely in Andrusov & Samuel (Eds.) 1984) has been well documented.

The lithological and lithofacial characteristics, mineral composition of detritic material as well as the type of synsedimentary volcanism (Vozárová 1981; Vozárová & Vozár 1981, 1988) permit us to interpret the original basin as a consequence of continental rifting in the post-collisional stage of the Variscan orogeny (Vozárová 1996). All the above mentioned data enable us to presuppose a sedimentary basin with a total length of 450 to 550 km and a considerable width from several to tens of km (Vozár 1977). The total thickness of the IG sequence at present is 2200 to 2800 m. As a consequence of tectonic transport, the basal part of the NBF is tectonically truncated. Therefore, the whole thickness of the former Pennsylvanian Hronicum basin filling is unknown. Based on the findings of redeposited older Pennsylvanian palynomorphs (Ilavská 1964) and rock fragments (Vozárová 1981), it may be assumed that the latest Kasimovian–Gzhelian NBF was formerly underlain by relative older strata perhaps of Moscovian age.

Besides the above mentioned features, lithology, stratigraphy, areal extent, thickness and incomplete preservation with

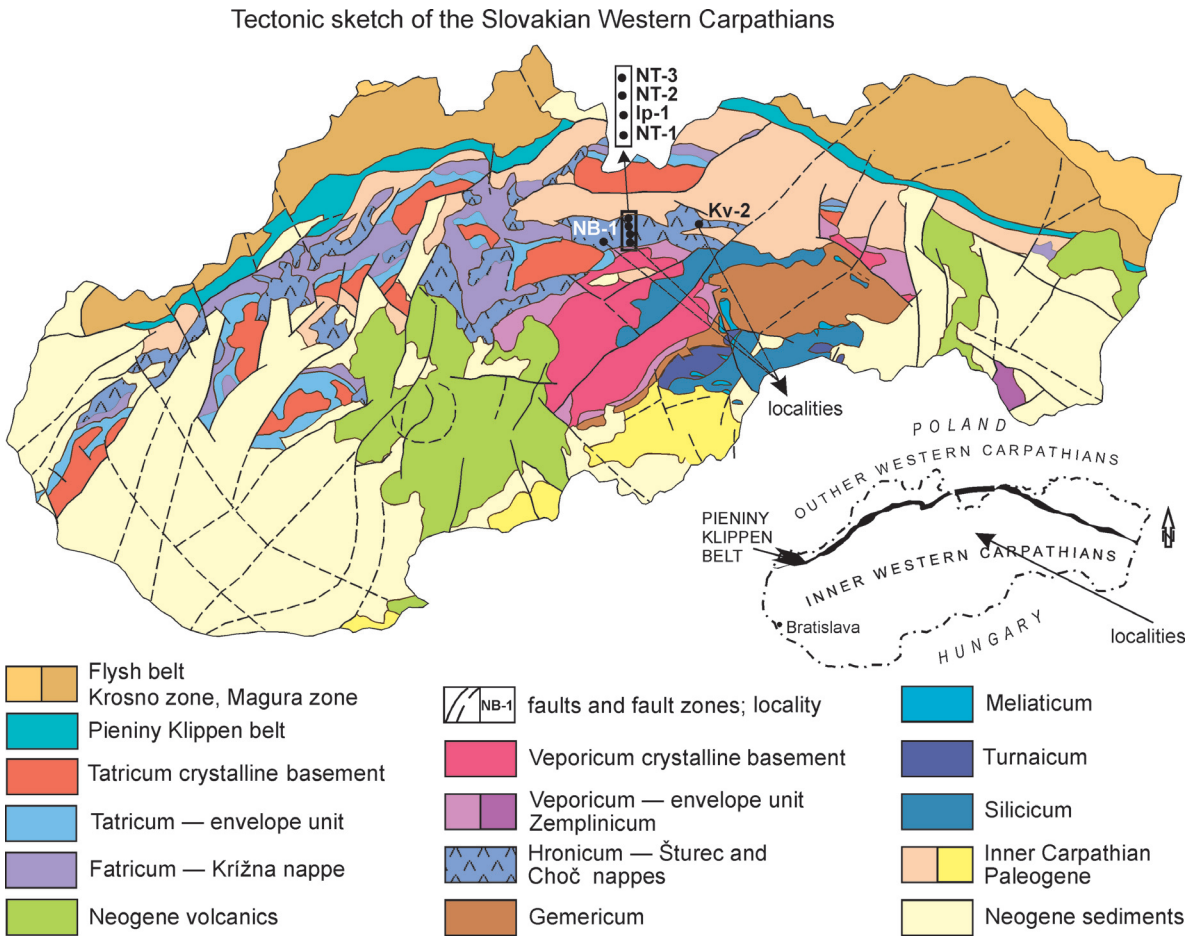

Fig. 1. Tectonic sketch of the Western Carpathians, Slovakia (Biely et al. 1996, modified by J. Vozár).

regard to tectonic amputation, the Upper Paleozoic of the Hronicum Unit differs from the other Upper Paleozoic occurrences in the Western Carpathians mainly in the presence of the characteristic basic volcanism. The presence of volcanic products is already evident in the upper horizons of the NBF (sporadic dacite effusions and volcanoclastics). They are a testimony of volcanic activity already in the beginning of rift-related basin formation. An essentially more intensive Permian basaltic andesite and basalt volcanism is concentrated into two distinct eruption phases (within the 1st and 3rd megacycles of the MF defined by Vozárová & Vozár 1981, 1988), which document distinct magmatic activity with manifestation of the linear type of volcanism connected with regional rifting of continental crust. Numerous effusions have been reported with thicknesses from 0.5 to 2.5 m of sheets of lava, traced at considerable distances (tens to hundreds of meters, sporadically also several km), as was documented in the Nízke Tatry Mts (Vozár 1974). This thickness testifies, besides other features, to the polyphase character and fluidity of the basic magma. Fluid structures, mainly in porous, amygdaloidal, but also fine-grained and porphyritic varieties are frequently documented at individual lava flows. So, together with evidences of transport directions in sediments and paleomagnetic measurements (Muška in Vozárová & Vozár 1988) it is possible to interpret the original south-north course and rift structure of the sedimentary basin. The low viscosity and adequate relatively low grade of explosivity are characteristic of mafic magmas and so the volcanoclastics are mostly of the ash and sand grain size. Lapilli with a maximum size of 2 cm were found only sporadically (Vozár 1971, 1974). Volcanoclastics are disproportionally less represented in relation to effusive bodies. The indications of deposition in a water environment were observed in the 1st eruption phase and in the basal part of the 2nd eruption phase. They are represented by fine lamination of ash tuffs, low-scale cross bedding, graded arrangement in small cycles (5–15 cm), wavy bedding, and oscillatory ripple mark lamination. There are frequent occurrences of thin (5–20 cm) layers of sediments and volcanoclastics between lava flows. The contacts of volcanic effusions with sediments and volcanoclastics are predominantly caustic-metamorphosed. Baked crust rich in Fe-pigment, epidote, chlorite, quartz, calcite veins, is usually 1 to 5 cm wide. The caustic contacts are uneven, marked by unequal penetration of lava into the plastic sediment, also with indications of contamination. Similarly, the contact of two effusions is also usually bordered by cinder structure and contamination from the side of younger effusion.

At several profiles, mainly in the upper part of the 2nd eruption phase, "pahoe-hoe" structures of lavas were observed. The disintegrated (brecciated) lavas, mainly observed in the 2nd eruption phase, are usually bordering the marginal or frontal parts of effusions. Even though not all structural marks documenting the character of volcanism are well preserved, the Permian volcanics in the Hronicum Unit are the best preserved paleovolcanics in the whole Western Carpathians especially from the structural point of view (Fig. 1). Compositionally, the basic rocks were described as rift-related continental tholeiites (Vozár 1997; Dostal et al. 2003).

Methods

Samples NT-1, 2, 3 for Sr and Nd isotope analyses were chemically prepared and measured in the Isotope Geochemistry Laboratory in the Institute of Geological Sciences of the Polish Academy of Science, Krakow. The analyses were made with a Multi-Collector Inductively Coupled Plasma Mass Spectrometer (MC-ICP-MS) Neptune. The samples were digested in three steps: firstly, with HF: HNO_3, secondly, with HNO_3 and finally, with HCl and HF, following the procedure described by Anczkiewicz et al. (2004) and Anczkiewicz & Thirlwall (2003). The samples were then dissolved in HCl for loading on cation exchange columns with AG50Wx8 resin (Anczkiewicz et al. 2004). Final separation of Sr was performed by Sr-spec resin (Peryt et al. 2010) and Nd by Ln-spec resin (Anczkiewicz & Thirlwall 2003). Nd isotopes were normalized to $^{143}Nd/^{144}Nd = 0.7219$ to correct for mass bias. The reproducibility of Nd standards over the period of analyses was $^{143}Nd/^{144}Nd = 0.512101 \pm 8$ (2 s.d. n = 3). Sr isotopes were normalized to $^{86}Sr/^{88}Sr = 0.1194$ to correct for mass bias. The reproducibility of Sr standards over the period of analyses was $^{87}Sr/^{86}Sr = 0.710261 \pm 8$ (2 s.d. n = 3). Isotope compositions of Ip-1 and Kv-2 samples were taken from Vozárová et al. (2007). They were also chemically prepared and measured in the Isotope Geochemistry Laboratory in the Institute of Geological Sciences of the Polish Academy of Science, Krakow. The εNd(0,t) values were calculated with parameters for CHUR $^{143}Nd/^{144}Nd = 0.512638$, $^{147}Sm/^{144}Nd = 0.1967$ (Jacobsen & Wasserburg 1980; DePaolo 1981).

All the dated samples were analysed for major and trace elements including rare earth elements in ACME Laboratories Ltd., Vancouver, Canada. Following a lithium metaborate/tetraborate fusion and dilute nitric digestion, major elements were determined by inductively coupled plasma (ICP) and trace and rare elements (REE) by inductively coupled plasma mass spectrometry (ICP-MS). The analytical accuracy was controlled using geological standards and is estimated to be within a 0.01 % error (1σ, relative) for major elements, and within a 0.1–0.5 ppm error range (1σ, relative) for trace elements and 0.01–0.05 ppm for REEs. Mineral analyses were carried out on a CAMECA SX-100 four-spectrometer electron microprobe in the Laboratory of Electron-Optical Methods of the State Dionýz Štúr Geological Institute in Bratislava using the standard procedures. The operating conditions were: 15 kV accelerating voltage, 20 nA focused beam current (φ 1–5 ηm) and 20–100 s counting time depending on the analysed elements.

Mineralogical and petrological characteristics

Dolerite sills and dykes: They cut exclusively the strata of the NBF. The thickness of individual sills varies from a few meters to more than 50 m (Fig. 2). The observed lateral extent of individual sills attains from tens of meters to ~500 meters. Subvertical dykes occur, but are not observed frequently. Thermal effects around intrusions are essentially developed in shales and siltstones, where hornfelsing, calcification, and silicification of the host rocks are observed. The

Fig. 2. Permian tholeiite andesite-basalts (Ipoltica valley section, northern slope of Nízke Tatry Mts). **a** — sheet of lava, 1st eruption phase, Malužiná Formation, **b** — detail of textures of 2nd eruption phase, Malužiná Formation, **c** — detail on thermal contact — basalt flow (upper part) and sediments of Malužiná Formation (lower part), **d** — laminated tuffs of Permian tholeitic basalts, Malužiná Formation, Hronicum, Ipoltica valley, Nízke Tatry Mts.

thickness of these altered zones attains up to 1–2 m, depending on the thickness of the dolerite bodies. The central parts of the sills and dykes are medium-grained and show doleritic, less commonly ophitic textures. The peripheral parts are fine-grained and have principally a microdoleritic texture.

The mineral composition of dolerites consists of plagioclase (45 vol. %), clinopyroxene (25 vol. %), Mg-hornblende (2 vol. %) fine-grained dark matrix, and opaque minerals (magnetite, titanomagnetite, ilmenite and rutile) (Fig. 3). The detected secondary minerals are albite, chlorite, actinolite, hydrogrossular, and occasionally pumpellyite-prehnite, described by Vrána & Vozár (1969). Ore minerals were described by Rojkovič (1977), Ferenc & Rojkovič (2001) and Olšavský & Ferenc (2002).

Clinopyroxenes in the less altered part of the dolerites are generally subhedral to euhedral and may occur as discrete crystals as well as aggregates. Cracks and fractures in clinopyroxenes may be filled with secondary minerals, mainly chlorite, fibrous actinolite and hydrogrossular. For the most part, the clinopyroxenes are fully replaced by the above mentioned secondary mineral association. Based on microprobe analysis (Table 1), the clinopyroxenes represent a Ca-Mg-Fe solid solution and can be expressed by the pyroxene quadrilateral system. According to IMA classification by Morimoto et al. (1988), the observed clinopyroxenes are situated in the diopside and augite range (Fig. 4). In general, the clinopyroxenes show an insignificant range of (Mg, Fe)↔Ca substitution. Commonly, during the initial stage of crystallization, the composition of clinopyroxenes is $Ca_{48-50}\,Mg_{42-43}\,Fe_{07-08}$. As differentiation proceeds on further cooling, the clinopyroxenes become relatively more iron-rich, $Ca_{45-46}\,Mg_{36-41}\,Fe_{13-19}$ in composition. These clinopyroxenes coexist marginally with magmatic Mg-hornblende (Fig. 3c).

The subhedral and anhedral crystals of clinopyroxenes are grouped radially or in an irregular mesh with lath-shaped crystals of plagioclases. In the volcanics of the 2nd eruption phase, clinopyroxenes often fill the interstices between the flow oriented laths of plagioclases. The selected chemical analyses of clinopyroxenes (Table 1, samples NT-2 and NT-3) confirm the presence of common rock-forming pyroxenes which can be expressed by the pyroxene quadrilateral system (Morimoto et al. 1988). In general, the basalt clinopyroxenes show an in-

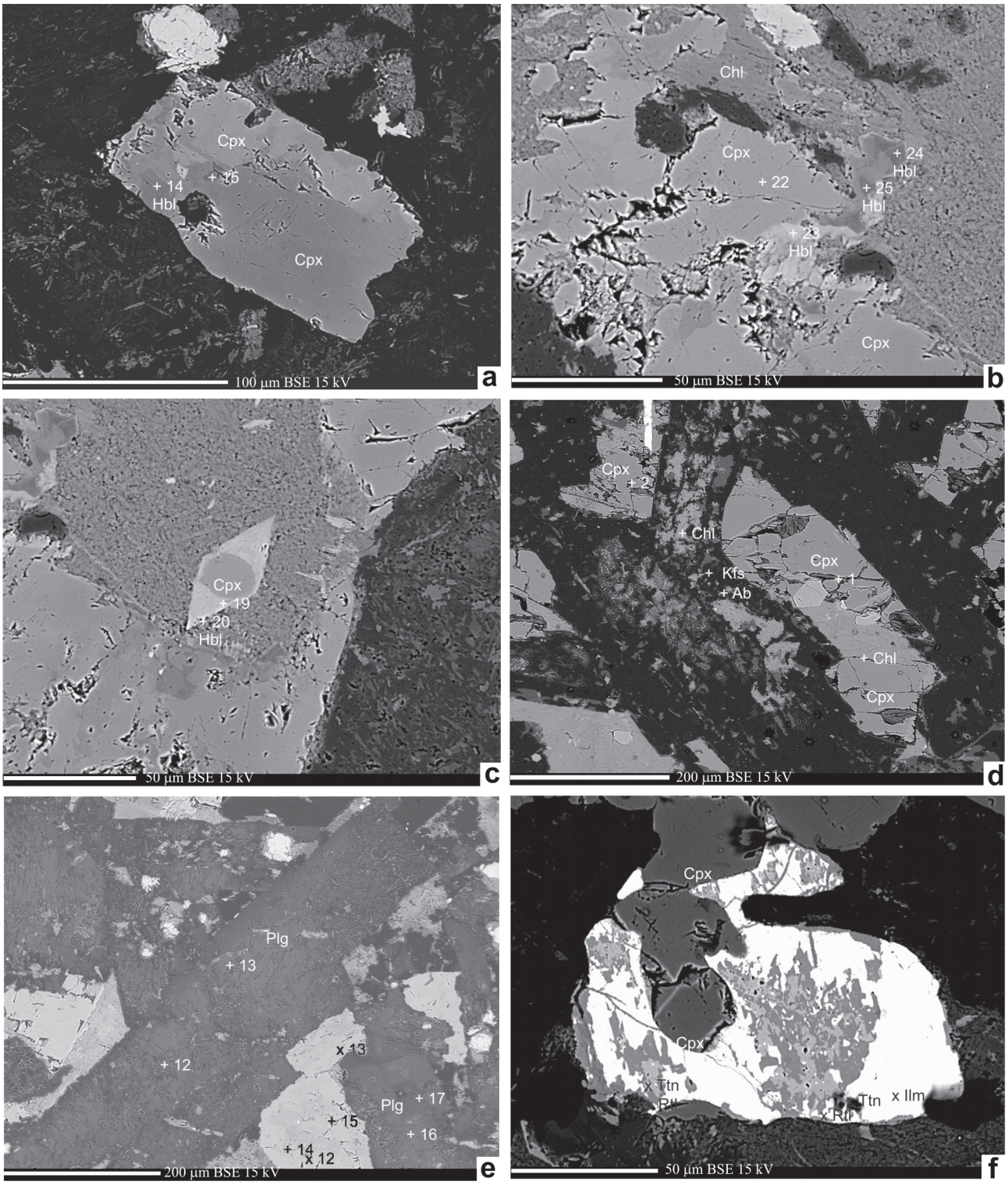

Fig. 3. BSE images of basalts from Malužiná Formation. **Cpx** — clinopyroxenes, **Hbl** — hornbledes, **Plg** — plagioclases, **Kfs** — K-feldspars, **Ab** — albites, **Chl** — chlorites, **Ttn** — titanites, **Rtl** — rutiles, **Ilm** — ilmenites, **+1–22** — numbers of analyses in Tables 1, 2, 3.

significant degree of (Mg, Fe)↔Ca substitution. The central part of these clinopyroxene phenocrysts from both volcanic horizons, is richer in Mg^{2+} ion, with a Ca_{45-50} Mg_{40-43} Fe_{09-14} variation The crystals of Mg-hornblendes (Table 2) are intergrown with the diopside, and are likely to have crystallized in equilibrium with more Fe-rich clinopyroxenes or immediately after their crystallization. This is documented by the enclosure of small Fe-rich diopside crystals within Mg-hornblende. The composition of this magmatic Mg-hornblende is characterized by 0.74–0.77 Mg ($Mg+Fe^{+2}$) ratios, 1.88–1.94

Table 1: Selected analyses of clinopyroxenes.

Sample	NT-1												NT-2								NT-3		
Analyses	1/1	2/1	4/1	5/1	8/1	11/1	15/1	19/1	21/1	22/1	2.1	3.1	4.1	10.1	26/1	27/1	28/1	29/1	17.1	18.1	23.1	32/1	34/1	35/1	38/1	39/1
SiO_2	50.77	52.96	51.51	50.48	51.78	52.73	52.59	50.67	53.64	52.08	51.58	52.10	51.98	51.84	51.38	51.99	51.64	51.83	51.51	51.40	51.42	51.57	51.76	51.57	51.74	51.02
TiO_2	0.90	0.18	0.82	0.96	1.47	0.14	0.21	0.99	0.04	0.38	0.92	0.14	0.39	0.58	0.53	0.40	0.47	0.44	0.37	0.45	0.91	0.87	0.92	0.89	0.96	0.99
Al_2O_3	2.11	0.59	2.32	2.26	1.88	0.53	0.68	2.42	0.19	1.09	2.09	0.57	0.95	1.23	1.05	0.65	0.77	0.87	0.67	0.86	1.34	1.42	1.49	1.68	1.28	1.66
Cr_2O_3	0.23	0.02	0.43	0.41	0.04	0.00	0.02	0.35	0.00	0.04	0.22	0.00	0.05	0.02	0.00	0.00	0.01	0.02	0.00	0.01	0.00	0.00	0.00	0.02	0.00	0.00
FeO	9.79	10.51	8.23	10.62	10.35	11.83	11.93	11.28	8.24	11.79	9.10	11.62	10.68	11.50	14.86	15.39	15.27	15.90	16.33	15.35	11.35	11.58	11.26	10.86	11.64	11.25
MnO	0.30	0.31	0.26	0.34	0.28	0.39	0.35	0.38	0.33	0.33	0.26	0.28	0.31	0.40	0.58	0.63	0.71	0.74	0.82	0.65	0.37	0.33	0.33	0.33	0.37	0.33
MgO	14.16	13.47	15.02	12.96	14.08	12.36	12.63	13.18	14.19	13.26	15.25	12.54	13.76	14.31	11.48	11.36	11.41	11.38	11.62	11.71	14.90	14.94	15.06	15.11	14.40	14.76
CaO	19.92	21.24	20.23	19.97	19.50	21.34	20.67	19.74	23.26	20.12	20.11	21.22	20.43	19.24	19.20	18.94	19.19	18.83	18.25	19.21	18.30	18.33	18.25	18.40	18.12	18.48
Na_2O	0.26	0.26	0.29	0.43	0.32	0.31	0.32	0.36	0.05	0.32	0.33	0.31	0.32	0.28	0.27	0.26	0.27	0.28	0.30	0.27	0.34	0.36	0.32	0.30	0.30	0.38
K_2O	0.01	0.01	0.00	0.00	0.00	0.00	0.00	0.00	0.01	0.01	0.00	0.01	0.00	0.00	0.00	0.00	0.00	0.01	0.01	0.00	0.00	0.01	0.00	0.01	0.00	0.00
Total	98.45	99.53	99.11	98.43	99.70	99.62	99.39	99.37	99.94	99.42	99.85	98.79	98.88	99.40	99.36	99.63	99.73	100.30	99.88	99.91	98.92	99.39	99.40	99.17	98.82	98.87
Formula based on 6 oxygens																										
Si	1.93	2.00	1.93	1.93	1.95	2.00	2.00	1.92	2.00	1.97	1.92	1.99	1.97	1.95	1.97	2.00	1.98	1.98	1.97	1.96	1.94	1.94	1.94	1.94	1.96	1.93
Ti	0.03	0.00	0.02	0.03	0.04	0.00	0.01	0.03	0.00	0.01	0.03	0.00	0.01	0.02	0.02	0.01	0.01	0.01	0.01	0.01	0.03	0.02	0.03	0.03	0.03	0.03
Al_{tot}	0.09	0.03	0.10	0.10	0.08	0.02	0.03	0.11	0.01	0.05	0.09	0.03	0.04	0.05	0.05	0.03	0.03	0.04	0.03	0.04	0.06	0.06	0.07	0.07	0.06	0.07
Al^{VI}	0.02	0.02	0.03	0.03	0.03	0.02	0.03	0.02	0.00	0.02	0.01	0.01	0.01	0.01	0.02	0.03	0.01	0.02	0.00	0.00	0.00	0.00	0.01	0.01	0.02	0.00
Cr	0.01	0.00	0.01	0.01	0.00	0.00	0.00	0.01	0.00	0.00	0.01	0.00	0.00	0.00	0.00	0.00	0.00	0.00	0.00	0.00	0.00	0.00	0.00	0.00	0.00	0.00
Fe'''	0.07	0.03	0.04	0.10	0.10	0.00	0.07	0.03	0.04	0.10	0.07	0.03	0.04	0.10	0.10	0.00	0.07	0.03	0.10	0.03	0.07	0.04	0.10	0.10	0.00	0.07
Fe''	0.08	0.07	0.06	0.04	0.05	0.37	0.08	0.07	0.06	0.04	0.08	0.07	0.06	0.04	0.05	0.49	0.08	0.07	0.05	0.46	0.08	0.06	0.04	0.05	0.37	0.08
Mn	0.01	0.01	0.00	0.01	0.00	0.01	0.01	0.01	0.00	0.01	0.01	0.01	0.00	0.01	0.00	0.02	0.02	0.02	0.00	0.02	0.01	0.00	0.01	0.00	0.01	0.01
Mg	0.50	0.55	0.54	0.44	0.45	0.70	0.50	0.55	0.54	0.44	0.50	0.55	0.54	0.44	0.45	0.65	0.50	0.55	0.45	0.67	0.50	0.54	0.44	0.45	0.81	0.50
Ca	0.57	0.62	0.63	0.51	0.50	0.87	0.57	0.62	0.63	0.51	0.57	0.62	0.63	0.51	0.50	0.78	0.57	0.62	0.50	0.79	0.57	0.63	0.51	0.50	0.74	0.57
Na	0.42	0.38	0.37	0.49	0.49	0.02	0.42	0.38	0.37	0.49	0.42	0.38	0.37	0.49	0.49	0.02	0.42	0.38	0.49	0.02	0.42	0.37	0.49	0.49	0.02	0.42
K	0.00	0.00	0.00	0.00	0.00	0.00	0.00	0.00	0.00	0.00	0.00	0.00	0.00	0.00	0.00	0.00	0.00	0.00	0.00	0.00	0.00	0.00	0.00	0.00	0.00	0.00
Jd	1.97	2.15	2.97	2.72	2.79	2.23	2.64	2.47	0.00	1.89	0.89	1.34	1.11	0.84	2.19	1.95	1.47	1.76	0.50	0.34	0.13	0.12	1.00	1.35	1.98	0.06
Ac	40.01	35.27	34.49	46.74	45.43	0.02	38.89	35.28	37.11	47.44	41.13	36.23	36.19	48.53	46.59	0.00	40.09	35.71	48.48	1.66	41.64	37.23	48.25	47.72	0.19	41.82
Aug	58.02	62.57	62.54	50.54	51.78	97.75	58.47	62.25	62.89	50.67	57.98	62.44	62.70	50.63	51.23	98.05	58.44	62.53	51.02	98.01	58.23	62.65	50.75	50.93	97.83	58.12

$(Ca+Na)_B$ 1.75–1.78 Ca_B and 0.16–0.13 Na_B. A part of the Mg-hornblende is of secondary origin and evidently derived from primary pyroxenes and replaced by Fe-actinolite through magmatic-hydrothermal activity in the final stage (Table 2; Figs. 3b,c, 5). Compositional variations of amphiboles from the studied doleritic rocks in terms of (Ca + Na + K = 1.99–2.17) and Si (7.18–7.94) atoms per formula unit (apfu) indicate igneous origins for both Mg-hornblende and Fe-actinolite (after Giret et al. 1980). Mg-hornblendes are secondarily altered mainly to chlorite and fibrous actinolite II. In this case, it could be assumed that amphiboles were partially affected also by a reaction with the metamorphic hydrothermal fluid alteration.

Plagioclases are dominant in the doleritic rocks, where they form idiomorphic prismatic crystals, typical of pericline and albite twinning. The chemical composition of plagioclases is shown in Table 3. The compositional ranges of plagioclases extend from An_{26} to An_{61}. Ca-rich phases are preserved only in the central part of the prismatic plagioclase crystals. The late-stage magmatic and metasomatic process replaced the composition of Ca-rich plagioclases towards Na-rich albite phase. In this respect, the albite phase forms the peripheral part of plagioclase crystals. Besides essentially Na and Ca variations, the plagioclases contain insignificant contents of orthoclase molecule, varying up to 6 molar percent (Table 3). Other ions which are present in very limited amounts include Fe^{+2} and Sr.

Basaltic andesites and basalts: Volcanics contain phenocrysts occupying around 30 vol. % of the rock trapped in variable amounts of volcanic glass. They are represented by plagioclases, clinopyroxenes, and opaque crystals, such as titanomagnetite, magnetite and ilmenite. Compared to the volcanics of the 2nd eruption phase, the volcanic rocks of the 1st eruption phase exhibit a higher grade of crystallinity. According to the relative proportion of crystals and glass, they demonstrate holocrystalline texture or a combination of holocrystalline and hypocrystalline textures, while the 2nd phase volcanics contain mostly hypocrystalline textures. Depending on the relative position within the individual flows, the volcanics of the 1st eruption phase demonstrate intergranular, porphyric, subophitic and ophitic textures. The 2nd eruption phase volcanics are more characteristic for intersertal and pilotaxitic textures.

Table 2: Selected analyses of amphiboles.

Sample	NT-1											
Analyses	**3/1**	**14/1**	**20/1**	**23/1**	**24/1**	**25/1**	**11**	**12**	**13**	**14**	**15**	**16**
SiO_2	51.19	49.66	51.71	50.65	48.67	55.86	51.14	49.51	49.02	48.32	49.11	49.45
TiO_2	0.37	2.07	0.05	0.43	0.04	0.05	0.45	1.98	1.34	1.46	1.41	1.08
Al_2O_3	2.15	5.11	0.92	1.60	7.24	1.74	3.04	5.31	4.96	5.58	5.13	5.32
FeO	22.79	11.91	25.22	25.70	12.04	7.55	14.88	11.81	12.80	12.41	11.75	11.51
MnO	0.89	0.23	0.78	0.82	0.17	0.17	0.24	0.23	0.20	0.26	0.25	0.19
MgO	7.70	15.22	6.61	6.31	15.86	19.84	14.23	15.37	14.94	15.10	15.31	16.05
CaO	11.74	11.52	11.87	11.76	11.32	12.20	11.30	11.38	11.08	11.28	12.40	11.32
Na_2O	0.22	1.18	0.22	0.19	1.58	0.40	0.58	1.24	1.46	1.52	1.04	1.38
K_2O	0.12	0.32	0.03	0.09	0.57	0.16	0.30	0.30	0.53	0.46	0.27	0.41
Total	97.16	97.23	97.42	97.57	97.49	97.97	96.16	97.11	96.34	96.40	96.66	96.70
Formula based on 23 oxygens												
Si	7.78	7.18	7.94	7.79	7.02	7.79	7.54	7.16	7.20	7.09	7.19	7.17
Al^{IV}	0.22	0.82	0.06	0.21	0.98	0.21	0.46	0.84	0.80	0.91	0.81	0.83
Sum T	8.00	8.00	8.00	8.00	8.00	8.00	8.00	8.00	8.00	8.00	8.00	8.00
Al^{VI}	0.17	0.05	0.10	0.08	0.25	0.07	0.06	0.06	0.06	0.06	0.08	0.08
Ti	0.04	0.23	0.01	0.05	0.00	0.01	0.05	0.21	0.15	0.16	0.16	0.12
Fe^{3+}	0.13	0.31	0.11	0.09	0.44	0.16	0.31	0.35	0.32	0.32	0.12	0.40
Mg	1.74	3.28	1.51	1.45	3.41	4.12	3.12	3.31	3.27	3.30	3.34	3.47
Fe^{2+}	2.77	1.09	3.12	3.21	0.89	0.64	1.44	1.02	1.19	1.14	1.28	0.91
Mn	0.11	0.01	0.10	0.11	0.01	0.00	0.01	0.01	0.01	0.02	0.02	0.01
Sum C	4.96	4.97	4.95	4.99	5.00	5.00	5.00	4.97	4.99	4.99	5.00	4.98
Mg	0.00	0.00	0.00	0.00	0.00	0.00	0.00	0.00	0.00	0.00	0.00	0.00
Fe^{2+}	0.00	0.04	0.00	0.00	0.12	0.08	0.08	0.06	0.07	0.07	0.03	0.08
Mn	0.00	0.01	0.00	0.00	0.01	0.02	0.02	0.01	0.01	0.02	0.02	0.01
Ca	1.91	1.78	1.95	1.94	1.75	1.82	1.78	1.76	1.74	1.77	1.94	1.76
Na	0.06	0.16	0.05	0.06	0.13	0.07	0.09	0.17	0.18	0.14	0.03	0.15
Sum B	1.98	2.00	2.00	2.00	2.02	1.99	1.97	2.00	2.00	2.00	2.02	2.00
Na	0.00	0.17	0.02	0.00	0.31	0.04	0.08	0.18	0.24	0.29	0.26	0.24
K	0.02	0.06	0.01	0.02	0.11	0.03	0.06	0.05	0.10	0.09	0.05	0.08
Sum A	0.02	0.23	0.02	0.02	0.41	0.07	0.13	0.23	0.34	0.37	0.31	0.31

Table 3: Selected analyses of plagioclases.

Sample	NT-1							NT-2		
Analyses	**12/1**	**13/1**	**16/1**	**17/1**	**18/1**	**33/1**	**36/1**	**37/1**	**40/1**	**41/1**
SiO_2	53.24	62.49	60.32	57.65	54.71	54.00	53.01	56.57	56.43	58.28
Al_2O_3	28.78	22.96	24.68	26.38	27.74	28.51	28.79	26.47	26.17	25.14
FeO	0.51	0.36	0.40	0.43	0.47	1.00	0.87	0.98	1.02	0.85
SrO	0.07	0.02	0.05	0.04	0.06	0.04	0.05	0.05	0.06	0.05
CaO	12.09	5.16	7.06	9.05	10.73	11.66	12.26	9.59	9.72	8.13
Na_2O	4.06	7.41	6.48	5.57	4.94	4.48	4.13	5.51	5.48	6.18
K_2O	0.30	1.00	0.54	0.38	0.32	0.24	0.22	0.34	0.37	0.46
Sum	99.04	99.39	99.52	99.50	98.98	99.93	99.33	99.53	99.25	99.10
Formula based on oxygens										
Si	2.46	2.82	2.74	2.63	2.51	2.48	2.45	2.59	2.59	2.67
Al	1.57	1.22	1.32	1.42	1.50	1.54	1.57	1.43	1.42	1.36
Ca	0.60	0.25	0.34	0.44	0.53	0.57	0.61	0.47	0.48	0.40
Na	0.36	0.65	0.57	0.49	0.44	0.40	0.37	0.49	0.49	0.55
K	0.02	0.06	0.03	0.02	0.02	0.01	0.01	0.02	0.02	0.03
X(Ca)	0.61	0.26	0.36	0.46	0.53	0.58	0.61	0.48	0.48	0.41
X(Na)	0.37	0.68	0.60	0.51	0.45	0.40	0.37	0.50	0.49	0.56
X(K)	0.02	0.06	0.03	0.02	0.02	0.01	0.01	0.02	0.02	0.03

Plagioclases are the dominant phenocrysts in all basaltic andesites and basalts and form typical lath-shaped crystals. They represent a maximum of 80 % in lavas of the 1st eruption phase and 65 % in lavas of the the 2nd eruption phase from the all phenocrysts. They usually show repeated albite and/or pericline twinning on a microscopic scale. The pericline and albite twinning often occur in one crystal. Selected chemical analyses of plagioclases document prevalent intermediate composition of the 1st eruption phase plagioclases, with An_{41-61} and a small content of orthoclase molecule (Or_{1-3}). The relatively more basic plagioclases were identified in the volcanics of the 2nd eruption phase, with An_{61-77}. In general, the plagioclases are optically homogeneous, but the variation of An component within the individual plagioclase crystals from more calcic core to more sodic rim indicates a continuous change in composition of plagioclase crystals with falling temperatures. Among the secondary alterations of plagioclases, saussuritization is prevalent. Fine-

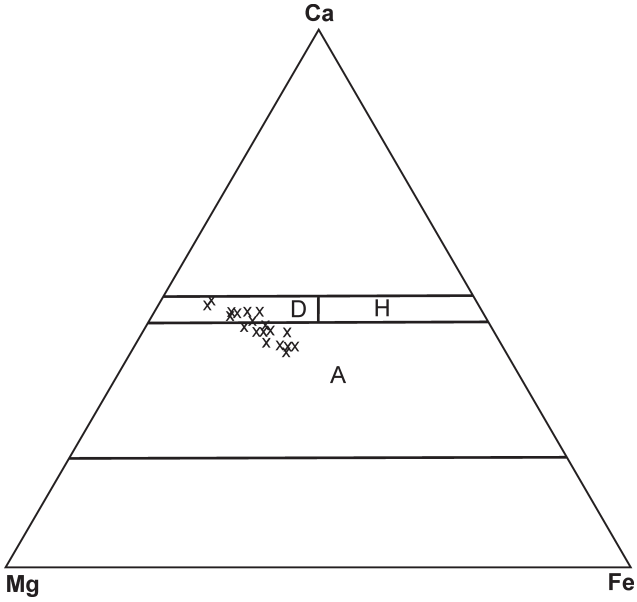

Fig. 4. Classification diagram of clinopyroxenes (Morimoto et al. 1988).

grained phylosilicates and occasionally pumpellyite were also detected. As a result of hydrothermal processes, the plagioclases were replaced by secondary albite and exceptionally, by K-feldspar.

As for accessory minerals, these rocks contain long-columnar crystals of apatite and oxides the latter are represented by titanomagnetite and ilmenite. The magmatic ilmenite is disintegrated to titanite and rutile in places.

Geochemistry

We classify our basaltic rocks on the basis of a TAS diagram (Fig. 6). The projection points of the analyses are lying in the field of trachyandesites and are located along the dividing line between alkali basalts and calc-alkali and/or tholeiitic basalts (Vozár 1977; Dostal et al. 2003). It is likely that their location was a result of a slight enrichment in alkalies during post-magmatic processes.

In order to make a more precise classification of the rocks under study and possible genetic interpretations, we used different discrimination diagrams (Figs. 7, 8). In the Nb:Zr/4:Y diagram (Fig. 7), the projection points of the analysed basalts are lying in the field of within-plate tholeiites, near the field of volcanic arc basalts. In the second diagram showing the dependence of contents Th:Hf/3:Ta (Fig. 8), the analyses of the studied rocks plot to fieldD, which corresponds to the composition of calc-alkali volcanic arc basalts. Another diagram (Fig. 9) allows us to make a more precise differentiation of these two basalt-originating environments. This diagram distinguishes three basic geotectonic environments: the field of volcanic arc basalts (subduction zone 1), the field of continental basalts and behind-arc basalts (2), and the field of ocean basalts (different types of mid-ocean ridge basalts (MORB 3)). In this diagram, the studied rocks are lying in the field of continental basalts, which partly overlaps with the field of volcanic arc basalts.

The REE normalized curve (Fig. 10) is rather flat with a slight enrichment in light REE, and almost no Eu anomaly is observed. To obtain better data on geochemical characteristics, we also used trace element normalization to the composition of the primordial mantle (Fig. 11). Compared to the

Table 4: Chemical composition of studied samples.

Sample	NB-1	NT-1	NT-2	NT-3
SiO_2	51.46	51.17	57.05	54.64
TiO_2	1.76	1.50	1.07	1.21
Al_2O_3	16.20	17.73	16.32	17.97
Fe_2O_3	9.38	8.83	9.89	7.05
MgO	4.98	5.18	2.12	3.15
CaO	6.88	7.50	2.77	7.60
MnO	0.18	0.15	0.24	0.10
Na_2O	5.09	3.70	6.62	4.41
K_2O	0.34	1.44	1.27	0.60
P_2O_5	0.31	0.25	0.60	0.24
LOI	3.20	2.20	1.80	2.90
Total	99.78	99.65	99.75	99.87
Ni	45	20	20	20
Sc	29	24	10	18
Ba	110	351	157	150
Co	27.6	27.5	14.5	23.4
Cs	1.4	1.9	2.1	0.3
Be	2	3	3	1
Ga	18.5	19	23	18.3
Hf	6.4	5.1	7.8	3.7
Nb	13.8	9.9	10.5	5.1
Rb	10.3	35.7	28.6	13.5
Sn	2	1	4	1
Sr	209.2	451.6	116.6	355.7
Ta	0.8	0.6	0.6	0.3
Th	5.4	3.3	4.5	2.8
U	1.4	0.9	2.2	0.9
V	189	192	34	154
W	2.3	0.5	8	11.3
Zr	236.1	186.2	336.9	149.2
Y	38.4	32.6	53.2	23.8
La	24.4	22.3	31.4	14.9
Ce	53.3	51.6	73.9	33.4
Pr	7.24	5.81	8.87	3.81
Nd	30.8	24.8	38	16
Sm	6.8	5.91	9.48	4.13
Eu	1.7	1.64	2.61	1.3
Gd	7.18	6.29	9.8	4.4
Tb	1.16	1.09	1.77	0.79
Dy	6.6	6.21	10	4.66
Ho	1.38	1.34	2.16	1
Er	4.06	3.99	6.55	2.9
Tm	0.6	0.56	0.93	0.4
Yb	3.72	3.36	5.82	2.41
Lu	0.56	0.52	0.93	0.42
Mo	5.5	0.5	1.5	0.4
Cu	22.5	19.4	14.2	2.3
Pb	5.6	14.1	41.8	3.5
Zn	59	70	248	51
Ni	44.5	15.7	1	10.7
As	1.4	1.1	4.9	1.3
Cd	0.1	0.1	0.5	0.1
Sb	0.1	0.6	0.3	0.1
Bi	0.1	0.1	0.1	0.1
Ag	0.1	0.1	0.1	0.1
Au	0.5	16	4	5.9
Hg	0.01	0.01	0.23	0.1

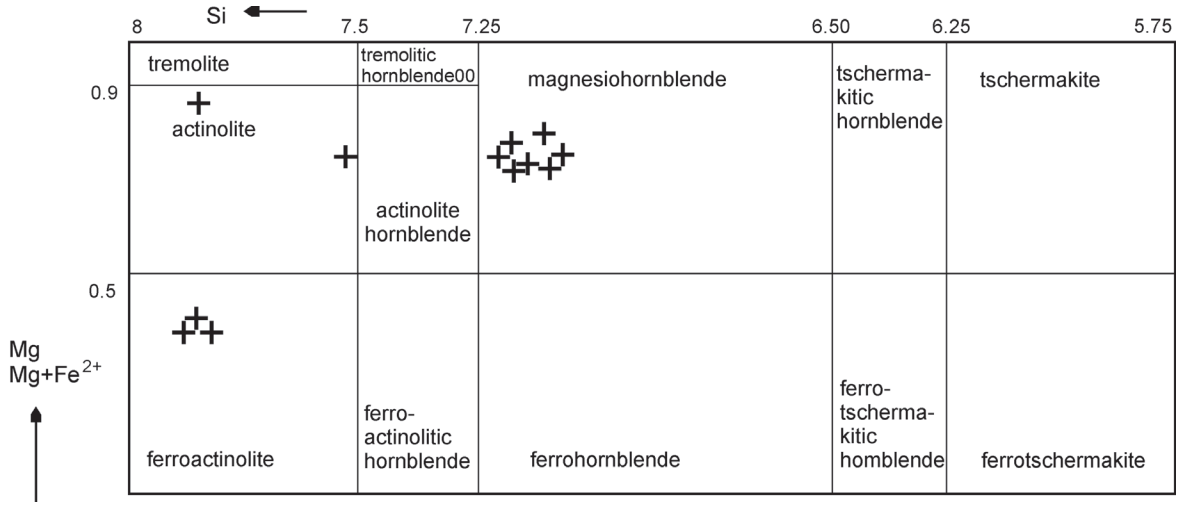

Fig. 5. Classification diagram of amphiboles (Leake et al. 1988).

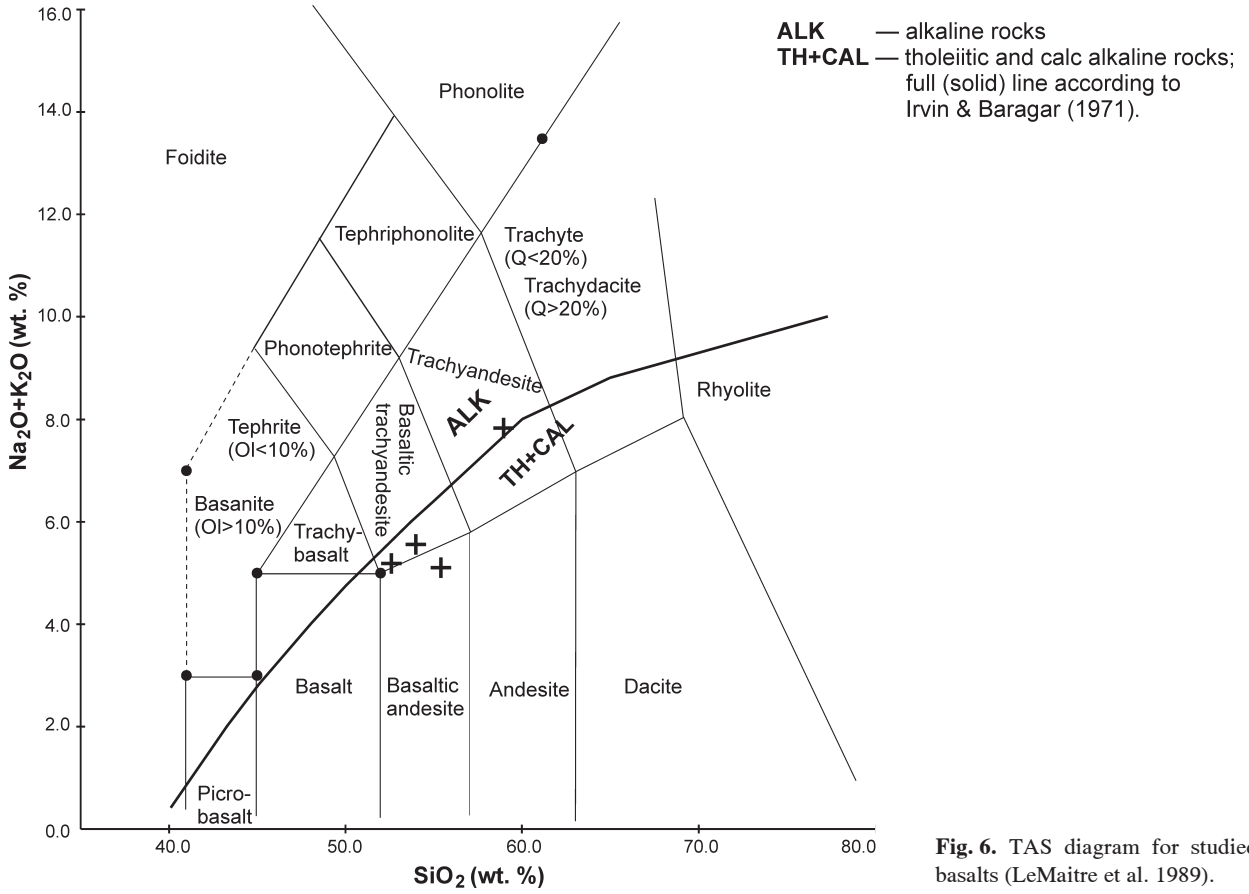

Fig. 6. TAS diagram for studied basalts (LeMaitre et al. 1989).

primordial mantle, most elements are enriched mainly Th, La and Ce. On the other hand, Ta, Nb and Sr are only slightly enriched and/or depleted.

In the studied Hronicum basic rocks, although the $mg^{\#}$ number [100 Mg/(Mg+Fe)] is low to moderate, ranging from 30 to 54, SiO_2 values are high (51–57 wt. %). According to Xu et al. (2001), the basalts can be classified as high-Ti (HT) and low-Ti (LT) basalts in terms of TiO_2 concentration (<2 % TiO_2) and <500 Ti/Y. In the studied samples, the TiO_2 content (1.07–1.76 wt. %) places the lavas among the low-Ti basalts. The Ti/Y ratios in the dolerite dykes as well as in the basaltic andesites and basalts of the first eruption phase are lower or close to (244–582) the recommended boundary 500 between HT and LT basalts. The Ti/Y value from the 2nd eruption phase basalt is much higher (630) and inclined to HT basalts. But all the studied Hronicum basic rocks have Fe_2O_3*

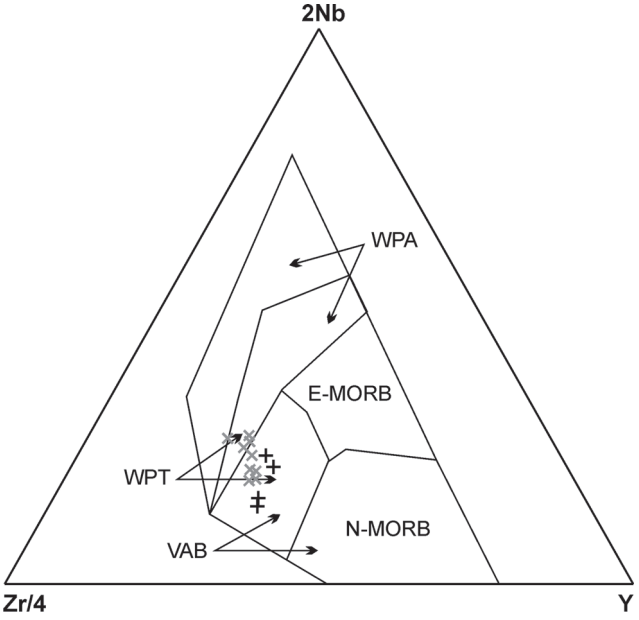

Fig. 7. The Nb-Zr-Y discrimination diagram for basalts (after Meschede 1986). The fields are defined as folows. **WPA** — within-plate alkali basalts, **E-MORB** — E-type MORB (Mid Ocean Ridge Basalt), **N-MORB** — Normal MORB, **VAB** — volcanic arc basalts, **WPT** — within-plate tholeiites, x — compared analyses from Dostal et al. (2003), + — analyses from Table 4.

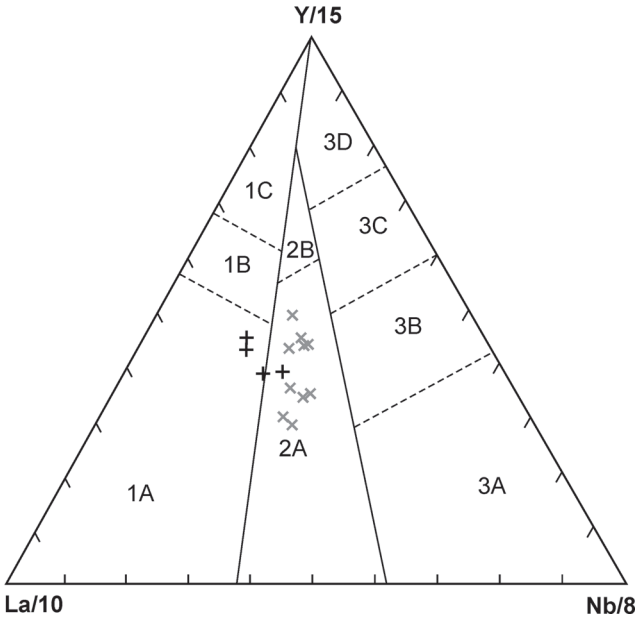

Fig. 9. The La-Y-Nb: discrimination diagram for basalts (after Cabanis & Lecolle 1989). Field 1 — volcanic arc basalts, field 2 — continental basalts and field 3 — oceanic basalts. The subdivision of the fields as follows: **1A** —calc-alkaline basalts, **1C** — volcanic arc tholeiites, **1B** — overlap between 1A and 1C, **2A** — continental basalts, **2B** — back-arc basin basalts, **3A** — alkaline basalts from intercontinental rift, **3B, 3C** — E-type MORB, **3D** — N-type MORB.

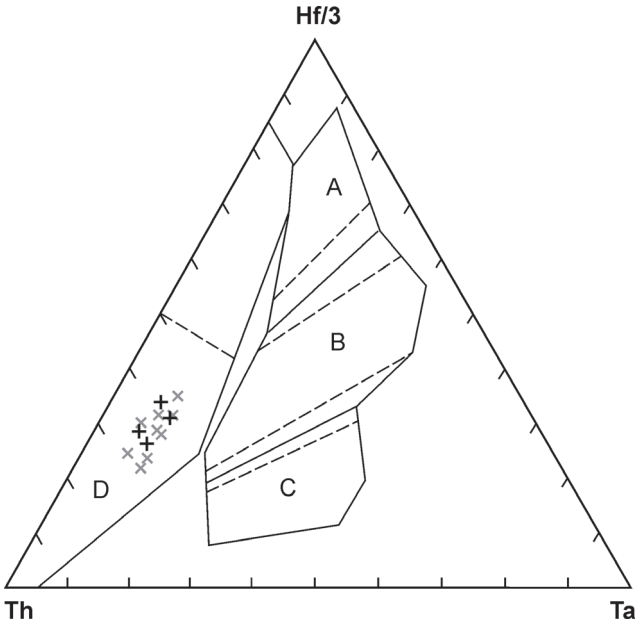

Fig. 8. The Th-Hf-Ta: discrimination diagram for basalts (after Wood 1980). The fields are defined as folows. **A**— N-type (normal) MORB (Mid Ocean Ridge Basalt), **B** — E-type MORB and within-plate tholeiites, **C** — within-plate alkali basalts, **D** — volcanic arc basalts. Island arc tholeiites plot in field D where Hf/Th 3.0 and calc-alkali basalts Hf/Th 3.0. The broken lines indicate transitional zones between basalt types.

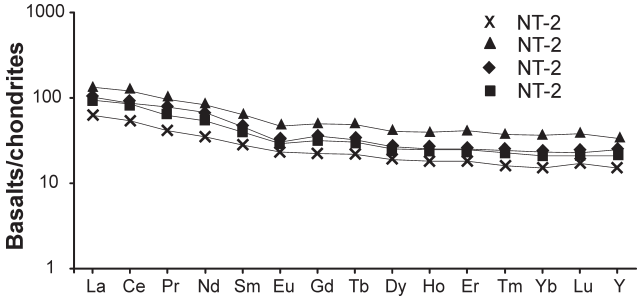

Fig. 10. REE concentration normalized to the chondrite composition (McDonough & Sun 1995).

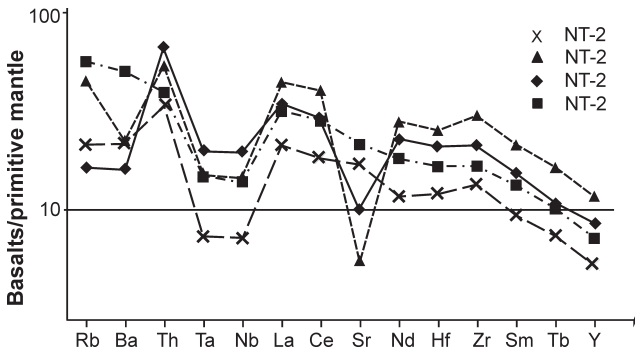

Fig. 11. Trace element concentrations normalized to the composition of the primordial mantle (McDonough et al. 1992).

< 12 wt. % and low ratios of Nb/La (0.3–0.6), which is more characteristic of LT basalts.

Isotopic data

Tables 5 and 6 show the results of isotopic analysis of Sr and Nd. The measured $^{87}Sr/^{86}Sr$ isotopic ratios in these samples are significantly different as a result of differences in $^{87}Rb/^{86}Sr$ between the samples. The Sr evolution plot shows that the intercept line for Sr evolution for basalt from the 1st intrusive phase (NT-2, IP-1) is closest to the expected extrusions age (about 290 Ma with an initial $^{87}Sr/^{86}Sr$ about 0.7054 (Fig. 12). Small differences in the calculated values of I_{Sr} (Table 5) for the analysed samples may document a partial Sr isotopic heterogeneity of the source (0.70435–0.70566), or a possible contamination of the original magma by crustal material. Moreover, the sample material could be altered to various degrees after the eruption, and this process may have changed the concentration of most incompatible elements such as Rb, Ba and K, because these elements are known for their high mobility.

For Nd analyses of the three samples, the calculated value for εCHUR (285) is positive for all samples and with only subtle variations. (Table 6) (Figs. 13, 14).

Discussion

The geochemical data we obtained can be compared with continental flood basalts (CFBs), whose extrusive ages are close to our samples. Siberian continental basalts have ages of 250.3 ± 1.1 Ma (Reichow et al. 2009; Shelnut & Jahn 2011) and the Emeishan flood basalt (~260 Ma) in southwestern China (Xu et al. 2001; Hou et al. 2011 and references therein), large igneous provinces which erupted during the Permian–

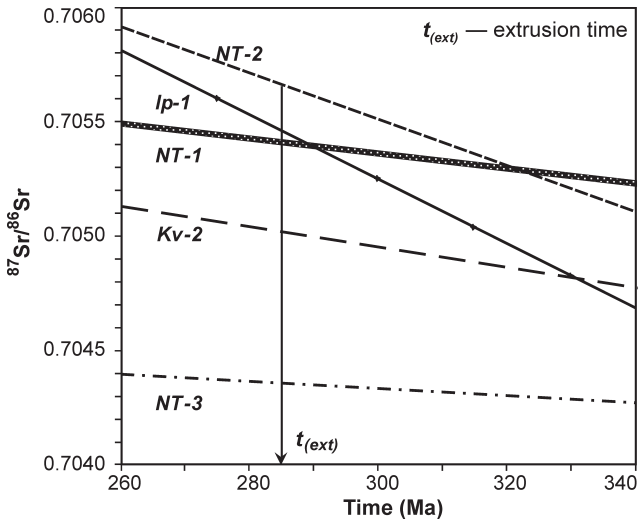

Fig. 12. Sr evolution diagram of samples analysed.

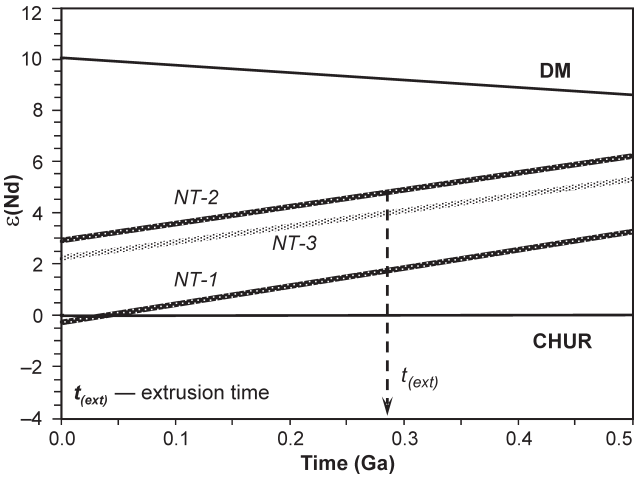

Fig. 13. ε(Nd) evolution lines in samples analysed with CHUR and DM sources.

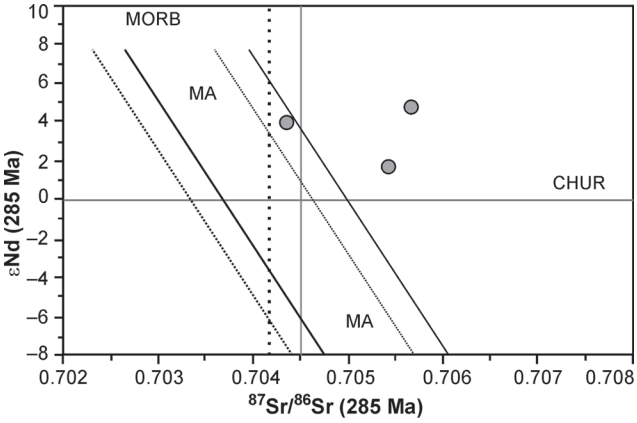

Fig. 14. The position of NT-1, NT-2, NT-3 sample points in εNd vs. $^{87}Sr/^{86}Sr$ plot. **MA** — mantle array, **dotted lines** — position at 285 Ma.

Table 5: Sr isotope analysis data from the studied samples.

	Rb (ppm)	Sr (ppm)	$^{87}Rb/^{86}Sr$	$^{87}Sr/^{86}Sr$	$I_{Sr}(285)$
NT-1	35.7	451.6	0.229	0.706340±11	0.705413
NT-2	28.6	116.6	0.710	0.708539±9	0.705661
NT-3	13.5	355.7	0.110	0.704797±9	0.704352
Ip-1*			0.992	0.709483±15	0.705461
Kv-2*			0.318	0.706302±11	0.705014

$I_{Sr}(285)$ — calculated initial $^{87}Sr/^{86}Sr$ in time of extrusion (285 Ma).

Table 6: Nd isotope analysis data from the studied samples.

	Sm (ppm)	Nd (ppm)	$^{147}Sm/^{144}Nd$	$^{143}Nd/^{144}Nd$	$I_{Nd}(285)$	$\varepsilon_{CHUR}(0)$	$\varepsilon_{CHUR}(285)$
NT-1	5.662	24.144	0.141772	0.512625±10	0.512361	–0.25	1.75
NT-2	9.118	38.297	0.145052	0.512787±11	0.512517	2.91	4.79
NT-3	4.171	16.961	0.148671	0.512752±18	0.512474	2.22	3.97

$I_{Nd}(285)$ – $^{143}Nd/^{144}Nd$.$\varepsilon_{CHUR}(285)$ — calculated parameters in time of extrusion (285 Ma).

Triassic period. Up to now, the origin of flood basalts, which are represented mainly by tholeiitic basalts, is highly disputable and a variety of models have been developed to explain their origin, but their genesis and sources are very complex. Generally, the following sources can be considered:

1) crustal contamination of MORB-like melts (Piccirillo et al. 1989; Campbell & Griffiths 1990; Arndt et al. 1993; Peate & Hawkesworth 1996; Campbell 2005);

2) melting of laterally heterogeneous subcontinental lithospheric mantle (Gallagher & Hawkesworth 1992; Sharapov et al. 2008);

3) mixing depleted and enriched mantle (Ellam & Cox 1991);

4) mixing enriched mantle melts and crust (DePaolo & Wasserburg 1979; Basu et al. 1998; Yan et al. 2007).

A subduction-related model has been presupposed by Ivanov et al. (2008) for the southeastern part of the Siberian Traps Large Igneous Province.

When comparing our data with those from the above mentioned areas, we can say overall consistency, even in the ($^{87}Sr/^{86}Sr$)t, and the εNd(t) values, reduced to the age of extrusion.

In the case of the Siberian CFBs, Wooden et al. (1993) concluded that the dominant volume of the erupted magma originated from an asthenospheric mantle plume, but none of the lavas are interpreted as representing asthenospheric melts. Moreover, the authors suppose that the dominant source of the erupted magma was a mantle plume. However, the compositions of the primary magmas were controlled by the thickness of the lithosphere, which influenced the depth of melting, the residual mineral assemblage, and the percentage of melting in the source region. The observed chemical and isotopic characteristics of the lavas indicate magma reservoirs through bulk assimilation and/or partial melting of crustal wall-rocks. Volumes of basaltic melt were produced directly from the continental lithospheric mantle beneath the Siberian craton (Wooden et al. 1993).

CFBs are likely to be a product of partial melting of mantle sources which represent primitive undifferentiated material and are clearly different from MORBs. This is a proof of crust contamination (DePaolo & Wasserburg 1979). For correlation, the Emeishan basalts (Xu et al. 2001; Xiao et al. 2004; Zhang et al. 2006; Liu & Zhu 2009 and references therein) are Permian–Triassic, they overlap the Permian carbonate formation and are covered by Triassic sedimentary sequences. Great CFB outpourings are genetically connected with "mantle plume activities". The composition of radiogenic isotopes of CFBs is out of the range of "plume sources" defined by oceanic island basalts (OIB). Only in cases when crust contamination can be excluded the lithospheric mantle can play an important role together with a significant contribution of plume materials (Chung & Jahn 1995). However, according to Hou et al. (2011) the Emeishan lavas cannot be classified by TiO_2 contents and/or Ti/Y ratios simply. Their high-Ti/lowTi characteristics are probably the results of different fractionating assemblages, so whether or not fractional crystallization of Fe-Ti oxides occurred. According to these authors this is the key factor that control the Ti abundance and Ti/Y ratios in the residual melts, and therefore, neither Ti-contents nor Ti/Y ratios can be reflect the nature of their mantle source (Hou et al. 2011).

In fact, our petrographic observations show that there are variable contents of Fe-Ti oxides in the MF basalts as the primary magmatic phase. Petrological modelling of Ganino et al. (2008) shows the possible derivation of low-Ti basalts from fractional crystallization of typical high-Ti basalts. These fractional crystallization processes may have been accompanied by contamination from subcontinental lithospheric mantle and/or continental crust (DePaolo 1981) and reflected by trace element ratios Th/Ta and La/Nb (Neal et al. 2002).

The major issue in the study of continental basalts is to identify their mantle source (Mahoney et al. 1982). The obtained data reflect a contamination of LIL-depleted magmas by two magmatic members; one is undoubtedly the continental crust and the other enriched mantle.

The MF basalts data suggest that the isotopic differences in the analysed samples $^{87}Sr/^{86}Sr$ (285 Ma)i, εNd(285 Ma) can be a result of 1) isotopic inhomogeneity of the source, 2) contamination of basalt magmas by crustal material. From this perspective, then we can assume that sample NT-3 (2^{nd} eruption phase) represents the least contaminated material and may correspond to the initial isotopic source.

The Sr evolution graph shows that during the extrusion of the 1^{st} eruption phase, the initial ratio $^{87}Sr/^{86}Sr$ was 0.7054, but for 2^{nd} eruption phase, it was 0.7051 (Fig. 12). With regard to the isotopic composition of Sr, we can assume an identical magmatic source. A higher ratio of $^{87}Rb/^{86}Sr$ (0.992) in the 1^{st} eruption phase is likely to have been caused by contamination of the extruding magma by crustal material. This trend is fully in line with the evolution of the Hronicum terrestrial rift with the progressing extensional regime on the cooling lithosphere, in which more links were made to the mantle along deep faults.

The geochemistry of the Hronicum basic rocks corresponds to the isotopic composition and implies source heterogeneity or a source mixing genetic model. Generally, the LT basalts are interpreted as a derivation from a shallower lithospheric mantle which underwent assimilation and fractional crystallization (Wooden et al. 1993; Arndt et al. (1993); Sharma 1997; Xu et al. 2001; Yan et al. 2007 and references therein). The Hronicum basic rocks are characterized by low Nb/La ratio, ranging from 0.56 to 0.33, and a negative correlation between Nb/La and SiO_2 which indicates that the evolved lavas underwent assimilation and fraction crystallization. This accounts for i) the nearly uniform major and trace elements and isotopic composition of LT lavas, ii) high ($^{87}Sr/^{86}Sr)_t$ ratios and iii) negative Nb-Ta anomalies.

The low values of the Th/Yb (0.77–1.45), Ta/Yb (0.10–0.21), Nb/La (0.33–0.56), Th/La (0.22–0.14) and Ta/La (0.02–0.03) ratios are characteristic of the Hronicum basic rocks and indicate a significant crustal contamination. Contrasting to these are the high Th/Ta ratios (5.5–9.3), which is in coincidence with the model of crustal contamination and characterizes the LT lavas (Lightfoot et al. 1993). Lightfoot et al. (1993) and Hawkesworth et al. (1995) used the La/Sm ratio (>3) for distinguishing of crustal contamination for the Siberian traps. In the Hronicum basic rocks these values are constantly higher than 3 (La/Sm = 3.3–3.8).

Similar results were reported by Dostal et al. (2003). Based on these authors, the Permian basic rocks of the

Malužiná Formation are compositionally rift-related continental tholeiites with enriched light REE patterns having $(La/Yb)_n$ ratios between 2 and 5.5 and with mantle-normalized patterns characterized by negative Nb-Ta anomalies. According to their chemical composition, Dostal et al. (2003) supposed a derivation of the Permian Malužiná Formation basic rocks from the subcontinental lithospheric mantle with a partial effect of crustal contamination.

In fact, the incompatible trace element patterns of the Hronicum basaltic rocks are likely to be related to a lithosphere mantle source and are dissimilar to the patterns of the oceanic basalts or plume-related basalts, also described by Dostal et al. (2003). These patterns are typical of many continental flood basalt provinces, such as Paraná, Columbia River plateau, Ethiopia, Siberian and Emeishan CFBs (Piccirillo et al. 1988; Dostal & Greenough 1992; Hooper & Hawkesworth 1993; Arndt et al. 1993; Sharma 1997; Kieffer et al. 2004; Reichow et al. 2009; He et al. 2010 and references therein). The good correlation with the Siberian traps is shown by the Siberian traps normalized patterns of the Hronicum basic rocks (Fig. 10b). These patterns are typical of subduction-related rocks as well as some within-plate continental tholeiites, which were not associated with contemporary subduction processes. The chemical composition of basalts suggests a possible later effect of older subduction-related processes that modified the lithospheric mantle, which then became the magma source (Hooper & Hawkesworth 1993). High Th/Nb ratio (>0.17) corresponding to primitive mantle is characteristic of subduction-related processes (Pearce 2008). In fact, the Hronicum basic rocks have a high Th/Nb ratio, ranging from 0.33 to 0.55, which indicates the subduction signature.

Composition data confirm the previous model of Dostal et al. (2003), which supposed the generation of parental magma for the Hronicum basic rocks from an enriched heterogeneous source in the subcontinental lithospheric mantle. This model is in concordance with the depositional model of the Malužiná Formation sedimentary basin, which originated in a rifted continental margin environment supplied from the continental crust and a dissected magmatic arc (Vozárová 1990, 1998). The Permian rift-related sedimentary basin of the Hronic Unit was situated in a foreland retro-arc setting on the continental crust. It was filled with clastic detritus derived from a dissected Mississippian magmatic arc and from the Permian syn-sedimentary volcanic centers, as is documented by the monazite ages (Demko & Olšavský 2007; Vozárová et al. 2014). The abundance of rhyolite-dacite detritus within the Hronicum Late Paleozoic clastic sediments entitles us to assume the bimodal type of volcanism. During the Cretaceous nappe stacking a large marginal part of the former sedimentary basin was tectonically cut off, which explains why only its distal parts with continental tholeiites have remained to the present fabric.

Conclusion

The relics of the Hronicum Late Paleozoic sequences represent only a part of the Late Carboniferous — Permian basin in the Inner Western Carpathians. Not only the character and distribution of sedimentary lithofacies, but also volcanics of fissural type provide evidence of this original basin as a regional rift system 450 km, perhaps more, in length. The mafic to intermediate products with a continental tholeiitic magmatic trend are a specific feature of this basin. The Permian volcanics correspond to within plate basalts. The chemical characteristics indicate that these volcanic rocks can be regarded as tholeiites related to deep (decompression) faults in an extensional regime with formation of a regional rift as a part of a continental margin, or a back-arc setting on continental crust. Chemical and isotopic data from the Hronicum basic volcanics suggest that the parental magma for the Hronicum basic rocks was generated from an enriched heterogeneous source in the subcontinental lithospheric mantle.

Acknowledgment: This study represents a partial output of the Grants: APVV-0081-10, APVV-0546-11, APVV-14-0038, VEGA 1/0095/12, 1/0141/015 and 1/0650/15. We are grateful to Jaromír Ulrych and Rastislav Demko for constructive comments on this paper and R. Anczkiewicz for kindly help with isotope analyses obtained in Isotope Geochemistry Laboratory (Polish Academy of Sciences, Kraków).

References

Allègre C.J. 2008: Isotope Geology. *Cambridge Press*., 1–512.

Anczkiewicz R. & Thirwall M.F. 2003: Improving precision of Sm-Nd garnet dating by H_2SO_4 leaching: A simple solution to the phosphate inclusion problem. *Geol. Soc. Spec. Publ*. 220, 83–91.

Anczkiewicz R., Platt J.P., Thirwall M.F. & Wakabayashi J. 2004: Franciscan subduction off to a slow start: evidence from high-precision Lu-Hf garnet ages on high grade-block. *Earth Planet. Sci. Lett*. 225, 147–161.

Andrusov D. 1968: Grundriss der Tektonik der Nördlichen Karpaten. *Slovak Acad. Sci. Publ. House*, Bratislava, 1–188.

Andrusov D., Bystrický J. & Fusán O. 1973: Outline of the structure of the West Carpathians. *Guide-Book Geol. Exc. X. Congr. CBGA*, *D. Štúr Geol. Inst.*, Bratislava, 5–44.

Andrusov D. & Samuel O. (Eds.) 1983–1985: Stratigraphic encyclopaedia of the Western Carpathians. 1st and 2nd vol. *Štúr Geol. Inst.*, Bratislava 1–40, 1–359 (in Slovak).

Arndt N.T., Czamanske G.K., Wooden J.I. & Fedorenko V.A. 1993: Mantle and crustal contributions to continental flood basalt volcanism. *Tectonophysics* 223, 39–52.

Basu A.R., Hannigan R.E. & Jacobsen S.B. 1998: Melting of the Siberian mantle plume. *Geophys. Res. Lett.* 25, 2209–2212.

Biely A. & Fusán O. 1967: Zum Problem der Wurzelzonen der subtatrischen Decken. *Geol. Práce, Spr.* 42, 51–64.

Biely A., Bezák V., Elečko M., Gross P., Kaličiak M., Konečný V., Lexa J., Mello J., Nemčok J., Potfaj M., Rakús M., Vass D., Vozár J. & Vozárová A. 1996: Explanation to geological map of Slovakia 1:500,000. *Geol. Survey of Slovak Republic, Dionýz Štúr Publishers*, Bratislava, 6–87.

Cabanis B. & Lecolle M. 1989: Le diagramme La/10-Y/15-Nb/8: un outil pour la discrimination des séries volcaniques et la mise en évidence des procésses de mélange et/ou de contamination crustale. *C. R. Acad. Sci*. 2, 2023–2029.

Cabanis B. & Thiéblemont D. 1988: La discrimination des tholéiites continetales des basaltes ariere-arc. Proposition a'un nouveau diagrame, le triangel Th-3* Tb-2* Ta. *Bull. Soc. Géol. France* 4, 927–935.

Campbell I.H. 2005: Large igneous provinces and the mantle plume hypothesis. *Elements* 1, 265–269.

Campbell I.H. & Griffiths R.W. 1990: Implication of mantle plume structure for the evolution of flood basalts. *Earth Planet. Sci. Lett.* 99, 79–93.

Chung S.L. & Jahn B.M. 1995: Plume — lithosphere interaction in generation of the Emeishan flood basalts at the Permian-Triassic boundary. *Geology* 23, 10, 889–892.

Demko R. & Olšavský M. 2007: The problem of rhyolite detritus in the Malužiná Formation. *Miner. Slovaca* 39, 4, *Geovestník*, 8–9 (in Slovak).

DePaolo D.J. 1981: Trace element and isotopic effects of combined wallrock assimilation and fractional crystallization. *Earth Planet. Sci. Lett.* 53, 184–202.

DePaolo D.J. & Wasserburg G.J. 1979: Neodymium isotopes in flood basalts from Siberian Platform and inferencies about their mantle sources. *Proc. Nat. Acad. Sci.,* USA, 76, 7, 3056–3060.

Dostal J. & Greenough J.D. 1992: Geochemistry and petrogenesis of the early Mesozoic North Mountain basalt of Nova Scotia, Canada. In: Ragland P. & Puffer J.H. (Eds.): Eastern North American Mesozoic magmatism. *Geol. Soc. Amer., Spec. Pap.* 268, 149–159.

Dostal J., Vozár J., Keppie J.D. & Hovorka D. 2003: Permian volcanism in the Central Western Carpathians (Slovakia): Basin-and-Range type rifting in the southern Laurassian margin. *Int. J. Earth Sci.* 92, 1, 27–35.

Ferenc Š. & Rojkovič I. 2001: Copper mineralization in the Permian basalts of the Hronicum unit, Slovakia. *Geolines, Acad. Sci. Czech Republic* 13, 22–27.

Gallagher K. & Hawkesworth C. 1992: Dehydratation melting and the generation of continental flood basalts. *Nature* 258, 57–59.

Ganino C., Arndt N.T., Zhou M.F., Gaillard F. & Chauvel C. 2008: Interaction of magma with sedimentary wall rocks and magnetite ore genesis in the Panzihua mafic intrusion, SW China. *Miner. Deposita* 43, 677–694.

Hawkesworth C.J., Lightfoot C.J., Fedorenko V.A., Bleke S., Naldrett J., Doherty W. & Gorbachev N.S. 1995: Magma differentiation and mineralisation in Siberian continental flood basalts. *Lithos* 34, 61–88.

He Q., Xiao L., Balta B., Gao R. & Chen J.Y. 2010: Variety and complexity of the late-Permian Emeishan basalts: reappraisal of plume-lithosphere interaction processes. *Lithos* 119, 91–107.

Hooper P.R. & Hawkesworth C.J. 1993: Isotopic and geochemical constraints on the origin and evolution of the Columbia River basalt. *J. Petrology* 34, 1203–1246.

Hou T., Zhang Zh., Kusky T., Du Y., Liu J. & Zhao Zh. 2011: A reppraisal of the high-Ti and low-Ti classification of basalts and petrogenetic linkage between basalts and mafic-, ultramafic intrusions in the Emeishan Large Igneous province, SW China. *Ore Geol. Rev.* 41, 133–143.

Ilavská Ž. 1964: Sporen und Hystrichospheritiden aus dem Karbon der Niederen Tatra. *Geol. Zbor. Geol. Carpath.* 15, 2, 227–232.

Irvin T.N. & Baragar W.R.A. 1971: A guide to the chemical classification of the common volcanic rocks. *Canad. J. Earth Sci.* 8, 523–548.

Ivanov A.V., Demonterova E.I., Rasskazov S.V. & Yasnigyna T.A. 2008: Low-Ti melts from the southeastern Siberian Traps Large Igneous Province: evidence for a water-rich mantle source? *J. Earth System Sci.* 117, 1–21.

Jacobsen S.B. & Wasserburg G.J. 1980: Sm-Nd isotope evolution of chondrites. *Earth Planet. Sci. Lett.* 50, 139–155.

Kieffer B., Arndt N., Lapierre H., Bastien F., Bosch D., Pecher A., Yirgu G., Ayalev D., Weis D., Jerram D.A., Keller F. & Meugniot C. 2004: Flood and shield basalts from Etiopia: Magmas from the African superswell. *J. Petrology* 45, 793–834.

Leake B.E., Woolley A.R., Birch W.D., Gilbert M.C., Grice J.D., Hawthorne F.C., Kato A., Kisch H.J., Krivovichev V.G., Linthout K., Laird J., Mandarino J., Maresch W.V., Nickel E.H., Rock N.M.S., Schumacher J.C., Smith D.C., Stephenson N.C.N., Ungaretti L., Whittaker E.J.W. & Youzhi G. 1997: Nomenclature of amphiboles. *Eur. J. Mineral.* 9, 623–651.

Leterrier J., Maury R.C., Thonon C., Girard I. & Marche L.M. l982: Clinopyroxene composition as a method of identification of the magmatic affinities of paleo-volcanic series. *Earth Planet. Sci. Lett.* 59, 139–154.

Lightfoot P.C., Hawkesworth C.J., Hergt J., Naldrett A.J., Gorbachev N.S., Fedorenko V.A. & Doherty 1993: Remobilisation of the continental lithosphere by a mantle plume: major-, trace elements, and Sr-, Nd-, and Pb- isotope evidence from picritic and tholeiitic lavas of the Noriľsk District, Siberian Traps, Russia. *Contr. Mineral. Petrology* 114, 171–188.

Liu Ch. & Zhu R. 2009: geodynamic significance of the Emeishan basalts. *Earth Sci. Frontiers* 16, 2, 052–069.

Lukeneder A. & Smrečková M. 2006: An Early Cretaceous radiolarian assemblage: palaeoenvironmental and palaeoecological implications for the Northern Calcareous Alps (Barremian, Lunz Nappe, Lower Austria). *Ann. Naturhist. Mus., Wien* 107A, 23–57.

MacDonald G.A. & Katsura T. 1964: Chemical composition of Hawaiian lavas. *J. Petrology* 5, 1, 82–133.

Mahoney J., Macdougall J.D., Lugmair G.W., Murali A.V., Das M.S. & Gopalan K. 1982: Origin of the Deccan Trap flows at Mahabaleshwar inferred from Nd a Sr isotopic and chemical evidence. *Earth Planet. Sci. Lett.* 60, 47–60.

McDonough W.F. & Sun S.-S. 1995: Composition of the Earth. *Chem. Geol.* 120, 223–253.

McDonough W.F., Sun S.-S., Ringwood A.E., Jagoutz E. & Hofmann A.W. 1992: Potassium, rubidium and cesium in the Earth and Moon and the evolution of the mantle of the Earth. *Geochim. Cosmochim. Acta* 56, 1001–1012.

Meschede M. 1986: A method of discriminating between different types of mid-ocean ridge basalts and continental tholeiites with the Nb-Zr-Y diagram. *Chem. Geol.* 56, 207–218.

Morimoto N., Fabries J., Ferguson A.K., Ginzburg I.V., Ross M., Seifert F.A., Zussman J., Aoki K. & Gottardi G. 1988: Nomenclature of pyroxenes. *Amer. Mineralogist* 73, 1123–1133.

Mullen E.D. 1983: $MnO/TiO_2/P_2O_5$: a minor element discriminant for basaltic rocks of oceanic environments and its implications for petrogenesis. *Earth Planet. Sci. Lett.* 62, 53–62.

Novotný L. & Badár J. 1971: Stratigraphy, sedimentology and metalogeny of the Late Paleozoicum of the Choč Unit in NE part of the Nízke Tatry Mts. *Miner. Slovaca* 3, 9, 23–90 (in Slovak, English summary).

Olšavský M. & Ferenc Š. 2002: Character of Permian volcanosedimentary sequences (Malužiná Formation) of the Hronicum unit at the NE part of Nízke Tatry Mts. *Geol. Carpathica, Spec. Issue,* 53 (only on CD-ROM, 2002), *Proceedings of the XVII Congress of Carpathian-Balkan Association*, Bratislava, 53/part 0.

Pearce J.A. 1982: Trace element characteristics of lavas from destructive plate boundaries. In: Thorpe R.S. (Ed.): Andesites. *J. Willey and Son*, Chichester, 525–548.

Pearce J.A. 2008: Geochemical fingerprints of oceanic basalts with applications to ophiolite classification and the search for Archean oceanic crust. *Lithos* 100, 14–48.

Pearce J.A. & Cann J. 1973: Tectonic setting of basic volcanic rocks determined using trace element analysis. *Earth Planet. Sci. Lett.* 19, 290–300.

Pearce J.A., Gorman B.E. & Bickett T.C. 1977: The relationship between major element chemistry and the volcanic rocks. *Earth Planet. Sci. Lett.* 36, 121–132.

Peate D.W. & Hawkesworth C.J. 1996: Lithospheric and asteno-

spheric transition in low-Ti basalts from Southern Paraná, Brasil. *Chem. Geol*. 127, 1–24.

Peryt T.M., Hryniv S.P. & Anczkiewicz R. 2010: Stroncium isotope composition of Badenian (Middle Miocene) Ca-sulphate deposits in West Ukraine: A preliminary study. *Geol. Quart.* 54, 465–476.

Piccirillo E.M., Comin-Chiaramonti P., Bellieni G., Civetta L., Marques L.S., Melfi A.J., Petrini R., Raposo M.I.B. & Stolfa D. 1988: Petrogenetic aspects of continental flood basalt — rhyolite suites from the Paraná Basin (Brasil). In: Piccirillo E.M. & Melfi A.J. (Eds.): The Mesozoic flood volcanism of the Parana Basin: petrogenetic and geophysical aspects. *São Paolo, IAG-SP*, 179–205.

Planderová E. 1973: Palinological research in the melaphyre series of the Choč — Unit in the NE part of Nízke Tatry between Spišský Štiavnik and Vikartovce. *Geol. Práce, Spr.* 60, *D. Štúr Geol. Inst*., Bratislava, 143–168 (in Slovak).

Planderová E. 1979: Biostratigraphy of the Carboniferous of the Choč nappe according palynology. *Geol. Práce, Spr.* 72, *D. Štúr Geol. Inst*., Bratislava, 31–61 (in Slovak, English summary).

Reichow K.M., Pringle M.S., Al'Mukhamedov A.I., Allen M.B., Andreichev V.L., Buslov M.M., Davies C.E., Fedoseev G.S., Fitton J.G., Inger S., Medvedev A.Ya., Mitchell C., Puchkov V.N., Safonova Yu., Scott R.A. & Saunders A.D. 2009: The timing and extent of the eruption of the Siberian Traps Large Igneous Province: Implication for the end-Permian environmental crisis. *Earth Planet. Sci. Lett.* 277, 9–20.

Rojkovič I. 1975: Geochemical characterization of U-Cu-Pb mineralization in the Permian of the Choč nappe in the Vikartovský chrbát area (the West Carpathians). *Geol. Zbor. Geol. Carpath.* 26, 105–114.

Rojkovič I. 1997: Uranium mineralization in Slovakia. *Acta Geol. Univers. Comen., Monogr*., Bratislava, 1–117.

Rojkovič I. & Konečný P. 2005: Th-U-Pb dating of monazite from the Cretaceous uranium vein mineralization in the Permian rocks of the Western Carpathians. *Geol. Carpathica* 56, 6, 493–502.

Sharapov V.N., Perepechko Yu.V., Perepechko L.N. & Rakhmenkulova I.F. 2008: Mantle sources of Permian-Triassic Siberian Traps (West Siberian Plate and Siberian Craton). *Russian Geol. Geophys.* 49, 492–502.

Sharma M. 1997: Siberian traps. In: Mahoney J.J & Coffin M.E (Eds.): Large igneous provinces: continental, oceanic and planetary flood volcanism. *Geophys. Monograph, Amer. Geophys. Union* 100, 273–296.

Shellnutt J.G. & Jahn B.-M. 2011: Origin of Late Permian Emeishan basaltic rocks from the Panxi region (SW China): Implications for the Ti-classification and spatial–compositional distribution of the Emeishan flood basalts. *J. Volcanol. Geotherm. Res.* 199, 85–95.

Sitár V. & Vozár J. 1973: Die ersten Makrofloren — Funde in dem Karbon der Choč — Einheit in der Niederen Tatra (Westkarpaten). *Geol. Zbor. Geol. Carpath*. 24, 2, 441–448.

Sun S.S. & Mc Donough W.F. 1989: Chemical and isotopic systematic of oceanic basalts: implication for mantle composition and processes. In: Saunders A.D. & Norry M.J. (Eds.): Magmatism in the oceanic basins. *Geol. Soc. London, Spec. Publ*. 42, 313–345.

Vozár J. 1971: Mehrphasig Character d. Permisch Vulkanismus in der Choč Einheit in d. Niedere Tatra Gebirge (Nízke Tatry). *Geol. Práce, Spr*. 55, *Geol. Úst. D. Štúra*, Bratislava, 131–137 (in German).

Vozár J. 1974: Structure of Permian Choč volcanites at the northern slope of the Nízke Tatry Mts. *Západ. Karpaty, Ser., Miner., Petrol. Geochem. Lož.* 1, *State Dionýz Štúr Geol. Inst*., Bratislava, 1–49 (in Slovak).

Vozár J. 1977: Magmatic rocks of tholeitic series in the Permian of the Choč Nappe of the Western Carpathians. *Miner. Slovaca* 9, 4, 241–258 (in Slovak, English summary).

Vozár J. 1997: Rift-related volcanism in the Permian of the Western Carpathians. In: Grecula P., Hovorka D. & Putiš M. (Eds.): Geological evolution of the Western Carpathians. *Miner. Slovaca–Monograph*, Bratislava, 225–234.

Vozárová A. 1981: Lithology and petrology of Nižná Boca Fm. *Západ. Karpaty, Sér. Miner. Petrol. Geochém. Metal.,* 8, *D. Štúr Inst. Geol*., 143–199 (in Slovak, English summary).

Vozárová A. 1996: Tectono-sedimentary evolution of Late Paleozoic basins based on interpretation of lithostratigraphic data (Western Carpathians; Slovakia*). Slovak Geol. Mag.* 3–4, 96, *D. Štúr Publ*., Bratislava, 251–271.

Vozárová A. & Vozár J. 1981: Lithostratigraphy of the Late Paleozoic sequences of the Hronicum. *Miner. Slovaca* 13, 5, 385–403 (in Slovak, English summary).

Vozárová A. & Vozár J. 1988: Late Paleozoic in West Carpathians. Monograph. *D. Štúr Inst. Geol.,* Bratislava, 7–314.

Vozárová A. & Vozár J. 1996: Terranes of West Carpathians–North Pannonian Domain. *Slovak Geol. Mag.* 1/96*, Dionýz Štúr Publ.*, Bratislava, 61–83.

Vozárová A., Kráľ J. & Vozár J. 2007: Sr isotopic composition in basalts of the Hronicum. *PETROS, Petrological Symposium, Abstracts Faculty of Natural Science, Geol. Inst. Slovak Academy of Sciences,* Bratislava 2007, 22 (in Slovak).

Vozárová A., Frank W.A., Kráľ J. & Vozár J. 2005: Ar^{40}/Ar^{39} dating of detrical mica from the Upper Paleozoic sandstones in the Western Carpathians (Slovakia). *Geol. Carpathica* 56, 6, 463–472.

Vrána S. & Vozár J. 1969: Mineral assemblage of pumpelyite-prehnite-quartz facies in Nízke Tatry Mts. *Geol. Práce, Spr.* 49, *D. Štúr Inst. Geol*., Bratislava, 91–99 (in Slovak, English summary).

Wood D.A. 1980: The application of a Th-Hf-Ta diagram to problems of tectonomagmatic classification and to establishing the nature of crustal contamination of basaltic lavas of the British Tertiary volcanic province. *Earth Planet. Sci. Lett.* 50, 11–30.

Wooden J.L., Czamanske G.K., FedorenkoV.A., Arndt N., Chauvel C., Bouse R.M., King B.-S.W., Knight R.J. & Siem D.F. 1993: Isotopic and trace-element constraints on mantle and crustal contributions to Siberian continental flood basalts, Noril'sk area, Siberia. *Geochim. Cosmochim. Acta* 57, 3677–3704.

Yan Z., Huang Zh., Xu Ch., Chen M. & Zhang Zh. 2007: Signatures of the Source for the Emeishan flood basalts in the Ertan area: Pb isotope evidence. *Chinese J. Geochem.* 26, 2, 207–213.

Xu Y., Chung S.-L., Jahn B.-M. & Wu G. 2001: Petrologic and geochemical constraints on the petrogenesis of Permian–Triassic Emeishan flood basalts in southwestern China. *Lithos* 58, 145–168.